Energy Equip. Sys./ Vol. 10/No. 3/Sep. 2022/ 255-269

ENERGY EQUIPSYS

Energy Equipment and Systems

http://energyequipsys.ut.ac.ir
www.energyequipsys.com

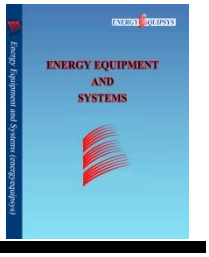

Presenting a new model for the analysis of infrared thermography of photovoltaic modules in order to determine the contribution of each module in the output power of photovoltaic power plants

Authors

Masoud Talaei[a*]
Saeid Rasuoli Jazi[a]

[a] Faculty of Mechanical Engineering, Islamic Azad University, Khomeinishahr Branch, Isfahan, Iran

ABSTRACT

In this study, a computational method for determining the contribution of each module in the output power of a photovoltaic power plant is presented and the results of that are compared with actual values. This method is based on infrared thermography. In other words, in this study, we are trying to develop a new model for analyzing the photovoltaic module thermography images through field measurements on several photovoltaic systems in Isfahan region. Since it is very important to precisely calculate the module surface temperature in this method, practical methods are presented to calculate the temperature accurately. Validation of these methods have been done by performing specific experiments. The results of this study show that for modules in which difference between maximum and minimum temperature in STC conditions is less than 10 ℃ and therefore classified in terms of temperature pattern in the healthy group, the calculation of power contribution of each module through this method is very close to the actual value and have an error below 2.8%.

Article history:

Received : 15 June 2021
Accepted : 17 July 2021

Keywords: Photovoltaic (PV) Module; Photovoltaic String; IR-Thermography; Hot-Spot, Glass Emissivity; Reflected Temperature.

Highlights

- A condition monitoring in photovoltaic modules using thermal imaging is proposed.
- Accurate calculation of the surface temperature of a photovoltaic module using Thermography is discussed.
- The contribution of each module in the output power of a photovoltaic string, is determined by Infrared thermography

1. Introduction

Photovoltaic power plants may generally suffer from various faults and defects during operation. In general, the most important methods of measurement and error detection in photovoltaic modules include: visual inspection, current-voltage curve (I-V), thermography, electroluminescence, ultraviolet fluorescence and signal transmission.

*corresponding author: Masoud Talaei
Faculty of Mechanical Engineering, Islamic Azad University, Khomeinishahr Branch, Isfahan, Iran
Email: masoud.talaei66@gmail.com

There are three different thermography methods for detecting errors in photovoltaic modules. These methods include steady state condition thermography, pulse thermography, and lock in thermography [1]. The most commonly used method is steady state condition thermography, which used in this article and henceforth referred to as thermography.

In recent years, several studies have been conducted to analyze the results of thermography and to identify possible defects in the modules. In addition, many articles have been published on this subject. Hoyer et al. [2] investigated the relationship between hotspot temperature and module power loss. Simon et al. [3] have investigated the detection of defects in a module through thermography at its different working points. Tsanakas et al. [4] have presented a classification of errors related to photovoltaic modules and how to detect them through thermography. Jaffery et al. [5] have introduced an algorithm for detecting the type of error in photovoltaic modules through thermography, also have suggested the type of required activities for troubleshooting. Álvarez-Tey et al. [6] analyzed the effect of environmental conditions (apparent temperature, light reflection, etc.) and imaging conditions (distance, angle, correct emission and etc.) on the accuracy of thermographic inspection of photovoltaic power plant. Takyi [7] provides an analysis of the relationship between visual inspections, current-voltage data, and infrared thermal images of photovoltaic modules.

In this study, at first it is explained that how to calculate the surface temperature of photovoltaic module by thermography, also the causes of hot spots in photovoltaic modules. In the following, the desired computational method is described and the experiments performed to validate this method, is explained. Finally, the results of the research and conclusions of the contents will be presented.

2. Infrared thermography

Infrared thermography is a non-destructive inspection technique that can be used as a non-contact method to diagnose some failures in photovoltaic modules. This inspection technique can be used from single modules to large-scale photovoltaic power plants. To use this, it must be ensured that the measurements are made under steady state thermal conditions.

2.1. calculation of the surface temperature of module by infrared thermography

Any object with a temperature above absolute zero emits infrared waves. The amount of radiation, according to Stephen Boltzmann's law, is proportional to the temperature of the body. In the infrared thermography, the radiation from the surface or object is detected by the infrared camera, accordingly the temperature of the object is calculated. Equation 1 shows the relationship between the emitted power and the object temperature [8].

$$P = \sigma A \varepsilon \left(T^4 - T_{amb}{}^4 \right) \quad (1)$$

In Eq.(1), "P" represents the radiative power emitted from the object, "σ" represents Stephen Boltzmann's constant and is equal to $5.67*10^{-8}$ $\frac{w}{m^2 k^4}$, "A" represents the area of the object, "ε" represents the emissivity of the object, "T" represents the absolute temperature of the object and "T_{amb}" represents the absolute temperature of ambient.

The radiation received by infrared camera includes three terms. These three terms are:

- Emissions from the object.
- Reflected emissions from ambient sources.
- Emissions from the atmosphere.

As shown in Fig. 1, the object (Section 2 in Fig. 1) emits thermal power (εW_{obj}) based on Eq.(1). In addition, the surrounding objects will emit to the object, and a percentage of this radiation will be reflected to the camera in proportion to the surface reflection coefficient (approximately equal to 1-ε). In proportion to the transmission coefficient (τ) of air between the object and the camera (Section 3 in Figure 1), a percentage of that emitted power, received by the camera. In addition, the air between the object and the camera can emits towards the camera in proportion to the ambient temperature. The amount of this emission (εW_{atm}) is approximately equal to (τ -1)× W_{atm}

For total received radiation power, can be written Eq.(2).

$$W_{tot} = \varepsilon\tau W_{obj} + (1-\varepsilon)\tau W_{ref} + (1-\tau) W_{atm} \quad (2)$$

And for the total power emitted from the object, can be written Eq.(3).

$$W_{obj} = \left(W_{tot} / \varepsilon\tau \right) - W_{ref} \left(1-\varepsilon / \varepsilon \right) - W_{atm} (1-\tau / \varepsilon t \quad (3)$$

In Eqs.(2) and (3), "τ" represents the transmission coefficient of the air between the object and the camera, which is calculated by FLIR tools software according to the distance and relative humidity.

"ε" represents the emissivity coefficient and is entered by the user in FLIR tools software.

"W_{ref}" represents the radiative power due to reflection of object, which is calculated by FLIR tools software according to T_{ref}

"W_{atm}" represents the radiative power due to the air between the object and the camera, which is calculated according to T_{atm}, by FLIR tools software.

Therefore, the temperature of the object can be calculated by using Eqs (1) and (3).

2.2. Cause of hot spots in photovoltaic modules

A hot spot is created in a photovoltaic module when, due to some anomaly or mismatch, the short circuit current of a damaged cell is less than the operating current of the other cells (for example, part of the cell goes out of work due to a cracking) and its ability to generate electric current is reduced. In this case, the damaged cell giving rise to reverse biasing (in other words, under pressure of other cells, it goes to the reverse bias region), thus dissipating the power generated by other cells as heat [10]-[11]- [12]. Fig. 2 shows the change in the working point of a damaged cell and its transfer to the reverse bias region. Therefore, there is a direct relationship between increasing temperature and power loss of a photovoltaic module [13].

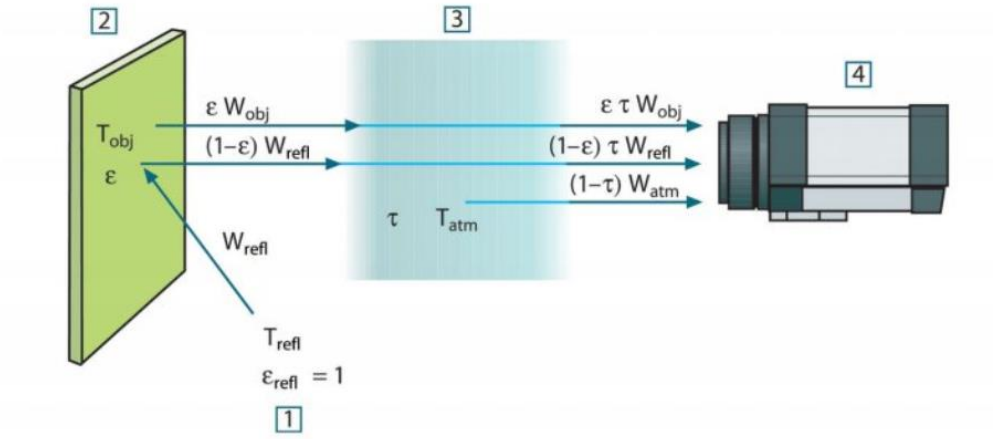

Fig. 1. Radiation received by infrared camera[9].

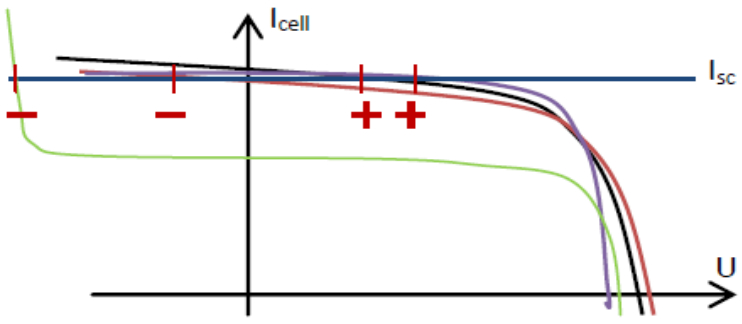

Fig. 2. I-V curve of 4 cells with different short circuit current [2].

As shown in Fig. 2, the cell corresponding to the green curve has a sharp drop in short-circuit current. This causes the cell to work in the reverse bias region and consume power instead of generating. The power consumed by this cell increases the temperature of the cell.

According to Eq.(1), it can be said that the power dissipated in the damaged cell is related to the increase in temperature of the corresponding cell compared to normal cells [14].

In addition, the temperature difference between the damaged cell and the other cells in a module is a function of the solar irradiance received by the module. Equation 4 shows the relationship between temperature difference and solar irradiance [15]:

$$\Delta T_2 = \Delta T_1 \left(G_2 / G_1 \right)^x \quad (4)$$

"Where" ΔT_i is the temperature difference between functional and non-functioning components under identical irradiance condition i;

G_i is the irradiance at condition i :

Index i = 1 is the value at actual (partial) irradiance.

Index i = 2 is the value at 100 % irradiance condition.

x is the exponential factor, considering different shapes of abnormalities.

For a point abnormality (point heat source with radial heat transfer) which is usually a few millimeters square and much smaller than a cell (for example, for a 6-inch silicon cell, a point abnormality is usually is less than 3 mm^2) the exponential factor x is usually between 1.5 and 1.8, and for extended area abnormality (usually the size of one or more cells) the exponential factor x is usually equal to 1 and indicates the linear dependence of temperature on the amount of irradiance. For impact of x see Fig. 3.

3. Computational method

This computational method is presented with the aim of determining the contribution of each module in the output power of a photovoltaic string, without the need to get the string out of circuit. In this computational method, the infrared thermal image is taken from all modules during operation and based on analyze of thermal images, the contribution of each module in the output power of the string (P_{mod}) is calculated. Due to the great importance of the emissivity coefficient and the apparent temperature of reflection, these two parameters are measured and calculated in practical ways. The steps of implementing this computational method are shown in Fig. 4 and are as follows:

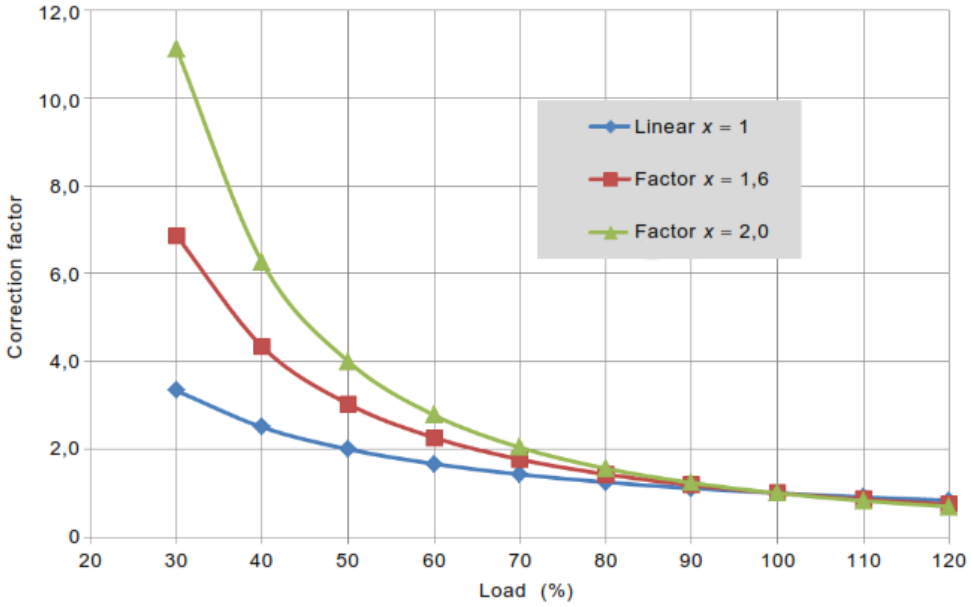

Fig. 3. Graphic representation of the correction factor for temperature differences to nominal irradiance conditions as a function of the relative irradiance [15].

1. Normal operating temperature of the cells ($T_{N.OP\ cell}$) is calculated.

Accurate calculation of normal cell temperature is very important because it is a reference for detecting high temperature points in the module and finally calculating the power loss caused by these points. Therefore, if there is an error in calculating the normal operating temperature of the cells, it will directly affect the results of the calculations. The normal operating temperature of the cells depends on many parameters such as the amount of solar irradiance, ambient temperature and wind speed. In this research, the average temperature of all module points is calculated by thermography and is considered as the normal operating temperature of the cells.

2. Temperature of the cells in open circuit conditions is calculated by Eq.(5) [16]:

$$T_{O.C\ cell} = T_{amb} + (T_{NOCT} - 20)\, G / 800 \quad (5)$$

"where" T_{amb} represents the ambient temperature (°C), G represents the amount of solar irradiance (W/m^2), T_{NOCT} represents the normal operating cell temperature in open circuit conditions (°C) and in the following situations:

- solar irradiance: 800 W/m^2
- Ambient temperature : 20 °C
- Wind speed : 1 m/s

This temperature indicates a high limit for the normal operating temperature of the cell.

3. If the average temperature of the module is close to $T_{O.C\ cell}$ ($|T_{N.OP\ cell} - T_{O.C\ cell}| < 3$°C), there is a possibility that the module be in open circuit condition or the module bypass diodes be turned on. In this case, the average temperature of the points corresponding to the junction box containing bypass diodes (T_{JB}) is calculated and compared with the average temperature of the module. If the junction box temperature is more than 5 °C above the module average temperature, the module is bypassed, otherwise the module is open circuit or connected in reverse polarity. In both cases, the contribution of module in output power of the string (P_{mod}) is zero.

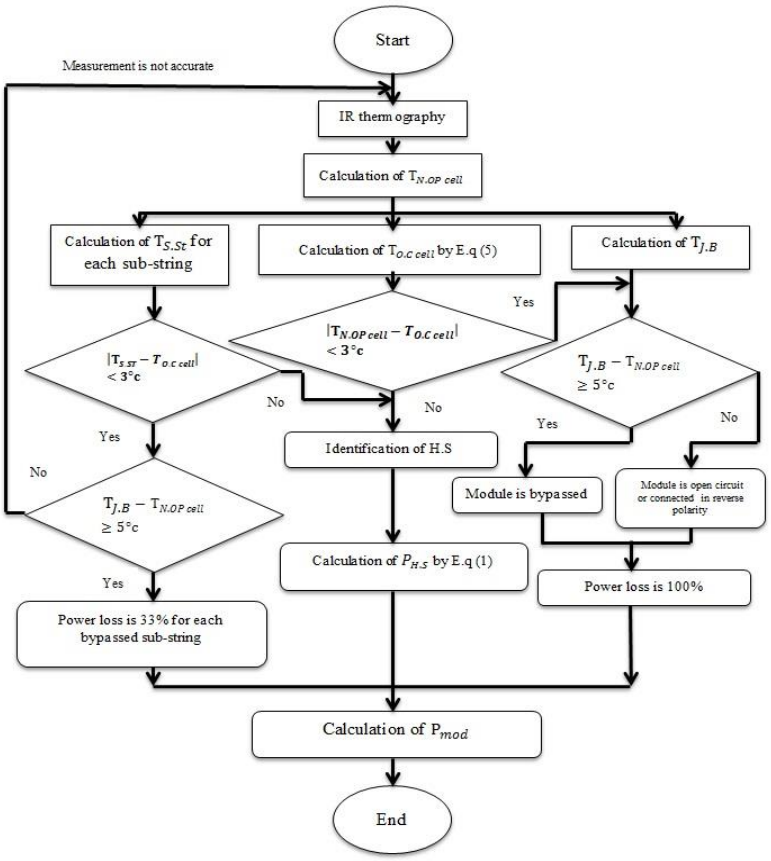

Fig. 4. Flowchart of the computational method for determining the contribution of each module in the output power of a photovoltaic string.

4. The temperature matrix of the module is divided into three parts (each part corresponds to a sub-string inside the module) and the average temperature of the three parts ($T_{S.St}$) are compared with each other and with $T_{O.C\ cell}$. If at least the temperature of one sub-string is higher than the average temperature of the module and close to $T_{O.C\ cell}$ ($|T_{S.ST} - T_{O.C\ cell}| < 3°C$), similar to step 3, the temperature of the junction box is measured. If the temperature of the junction box is also high, the corresponding bypass diode is turned on and the related substring is bypassed. In this case, we will have 33% power loss in the module for each bypassed sub-string.

5. In order to estimate the general conditions of the module, the temperature difference between the maximum and minimum temperature points in the module is calculated through a specific program written in Matlab software or the tools available in FLIR Tools software. This temperature difference is standardized by Eq. (4), or in other words, the amount of temperature difference under STC conditions (ΔT_{STC}) is calculated. After calculating this temperature difference, the modules are classified as follows [17]:

- If ΔT_{STC} < 10 °C the module is intact.
- If 10 °C < ΔT_{STC} < 20 °C the module must be monitored and the exact amount of power loss should be calculated through the curve.
- If ΔT_{STC} > 20 °C the module is damaged.

6. The temperature of each points of module (T_P) is compared with the average temperature of the module trough a specific program written in Matlab software. The points where temperature is more than the average temperature of the module ($T_P - T_{N.OP\ cell} > \boldsymbol{T_{margin}}$ and $\boldsymbol{T_{margin} = 3\ °c}$) are identified as hot spots (H.S) and the power loss caused by each point ($P_{H.S}$) is calculated by Eq.(1). The power loss of each module is equal to the total power loss of the respective hot spots.

7. Based on the amount of power loss estimated for each module in the previous step, the contribution of each module in the output power of string (P_{mod}) is calculated.

4. Test of proposed computational method

The experiments in this research were performed with two objectives of accurate measurement of the temperature of the module points and validation of the computational method. The following equipment were used in these experiments.

- Multi meter equipped with DC clamp and temperature sensor.
- solar irradiance measuring device equipped with an ambient temperature sensor and a contact sensor for measurement of module and cell surface temperature (Benning SUN)
- Infrared camera (FLIR one pro)
- PV analyzer (Benning PV2)

In addition, in order to analyze the data and information obtained from the experiments, the following softwares were used.

- FLIR Tools software
- MATLAB software
- SOLAR MANAGER software

4.1. Experiments for accurate calculation of the module temperature

Accurate calculation of the module temperature requires accurate calculation of the apparent reflectance temperature (T_{ref}) and the emissivity of the module surface. In this research, in order to accurate calculation of the T_{ref}, a device called lambert radiator was used. In order to test the accuracy of calculations based on the temperature of the lambert radiator, one of the modules installed in a rooftop system in Isfahan was selected. This module was polycrystalline type and had 2.5 years of operation. As shown in Fig. 5, in order to measure the T_{ref}, the lambert radiator was located near the module and the contact temperature sensor was mounted on the back of the module at the location of the 6/D cell. Matrix for cell identification can be seen in Appendix C.

Environmental conditions and configuration and location of thermographic camera was in accordance with Table 1.

In this experiment, the temperature of the cell is calculated by FLIR tools software for the emissivity between 0.8 and 0.92 and for 3 T_{ref} ($T_{ref} = T_{lam} = 3.9°c$, $T_{ref} = T_{amb} = 24°c$ and $T_{ref} = T_{sky} = 20°c$). The results of calculations are shown in Fig. 6.

Table 1. Experimental outline to determine the most accurate T_{ref}.

Experiment No : 18	**Module type: shinsung310w-polycrystaline**			**Location of the cell : 6/D**	
Environmental conditions					
Cloud coverage (octa)	Wind speed (Bft)	Solar irradiance (W/m2)	Ambient temp (°C)	shading	Module cleanliness
0	2	800	24	no	Clean
Configuration and location of thermographic camera					
Angle between the camera and the module surface (degree)	Distance between camera and cell (m)	Tilt of module (degree)	Current of module (A)	thermal stability (min)	
92	4	30	7.2	30	

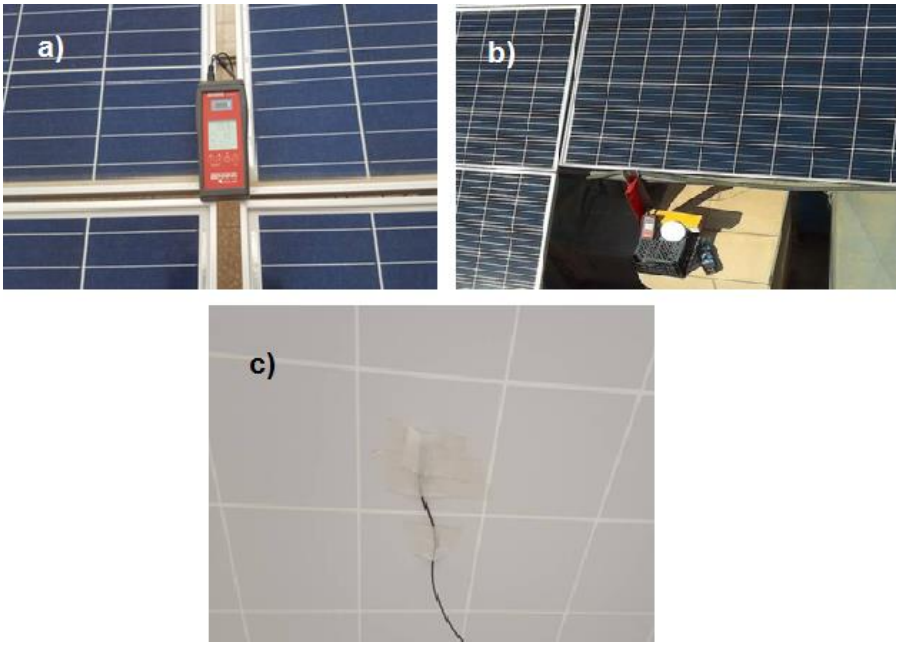

Fig. 5. a) location of solar irradiance measuring device, b) location of lambert radiator, c) location of contact sensor for measurement of cell (D/6) temperature

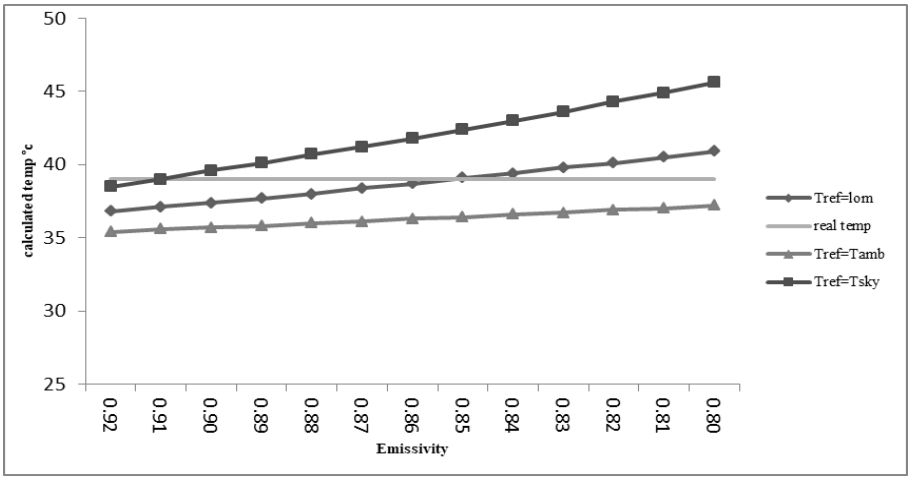

Fig. 6. Temperature calculated for different emissivities.

From the curves presented in Fig. 6, it can be concluded that for calculation of the temperature, use of a lambert radiator is the most accurate way to measure T_{ref}.

In order to determine of the emissivity of the photovoltaic module, a field experiment was performed. In this experiment, the angle of incidence was 90°, T_{ref} was set equal to the temperature of the Lambert radiator, and the temperature of the desired cell (D/6) was calculated by FLIR Tools software for different emissivities. The module under test is shown in Fig. 7.

In this experiment, environmental conditions and configuration and location of the thermographic camera was in accordance with Table 2.

In this experiment, the desired cell temperature was calculated for different emissivities and compared with real temperature (from contact temperature sensor). The calculated temperature curve relative to the emissivity and the real temperature can be seen in Fig. 8.

Therefore, according to the curve in Fig. 8, the most accurate emissivity for the module top glass is equal to 0.85. This value is considered as the actual emissivity of the module surface in later experiments.

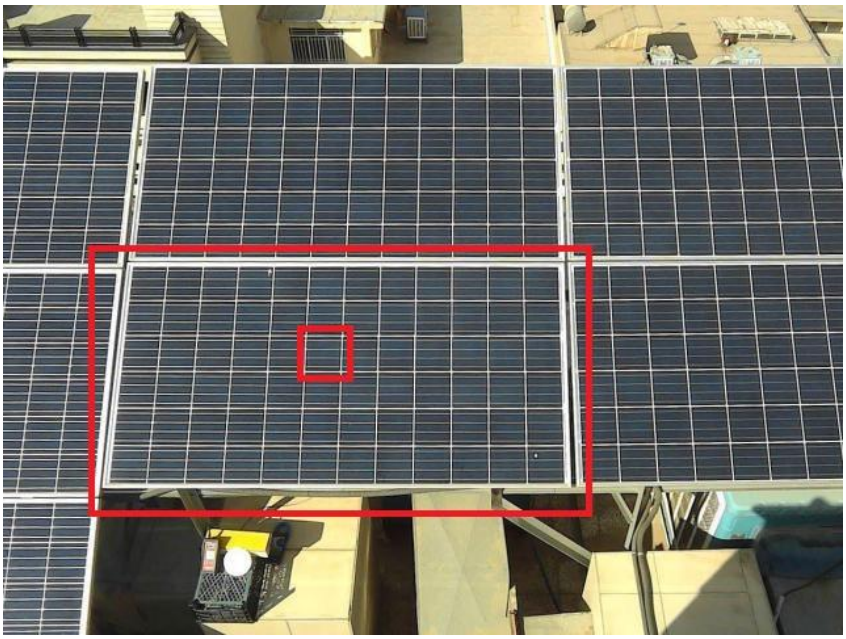

Fig. 7. The module under test and desired cell (D/6) for experimental determination of emissivity.

Table 2. Experimental outline to determine emissivity.

Experiment No : 18	**Module type: shinsung310w-polycrystaline**				**location of the cell : 6/D**
Environmental conditions					
Cloud coverage (octa)	Wind speed (Bft)	Irradiation (W/m2)	Ambient temp (°C)	shading	Module cleanliness
0	2	800	24	no	Clean
Configuration and location of the thermographic camera					
Optimum camera height (m)	Minimum camera height (m)	distance between the camera and the cell under test (m)	Tilt of module (degree)	The height of the camera relative to the lowest side of the module(m)	Horizontal distance to the module (d)
5.5	2.4	4	30	2.7	2

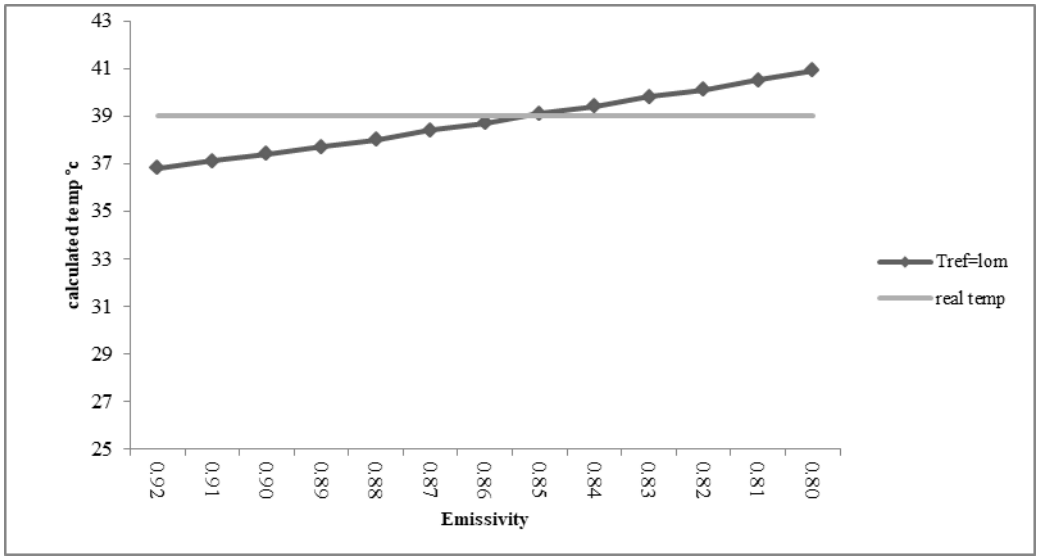

Fig. 8. Claculated temperature for different emissivity.

4.2. Experiments performed to validate the computational method

In order to check the accuracy of the computational method, one of the strings installed in a 100 kw power plant in Isfahan was selected. In this power plant, 400 polycrystalline modules with capacity of 270 w have been used and arranged in 22 strings. The modules had 2.5 years of operation. To select the best string for test, at first, the I-V curve of all strings was measured and one of the strings that had more power degradation was selected. According of test results, string number 9 was selected. This string has 20 polycrystalline modules and its I-V curve is shown in Fig. 9.

As shown in Fig. 9, slope of the STC performance curve near the short circuit current point is more than the NOM curve. This difference indicates a mismatch between the modules in this string.

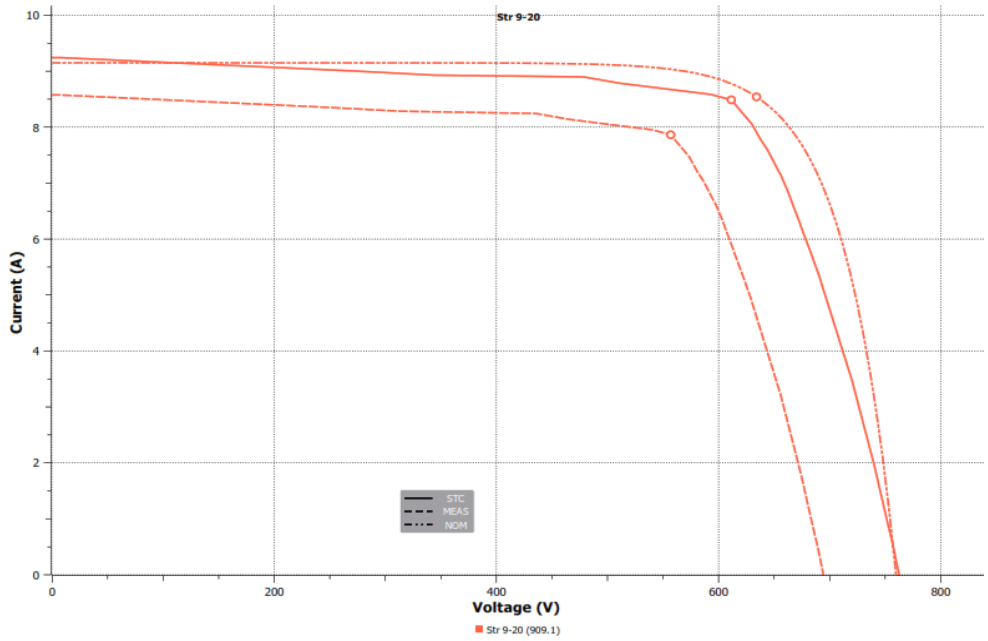

Fig. 9. I-V curve of string number 9.

After selecting string number 9 for detailed testing, an infrared thermal image was taken from each modules of this string. Fig. 10 shows part of this test. The specific parameters and requirements (appropriate angle and distance between camera and module and so on) was also taken into account during thermography. Immediately after completion of the thermography, the string was disconnected and I-V curve measurement was performed. In I-V curve measurement, string number 9 and each of its modules were measured separately. In this experiment, environmental conditions and configuration and location of the thermographic camera was in accordance with Table 3.

The I-V curve of modules are shown in Fig. 11 and the performance parameters of those are shown in table A.1.

For all modules in string number 9, the difference between maximum and minimum temperature in STC conditions is less than 10 °C and therefore classified in terms of temperature pattern in the healthy group. Therefore, as can be seen in table B.1, the results of the computational method and the I-V curve are very close. The maximum error is in case $T_{margin} = 0$ °C and is equal to 0.14 (equivalent to 2.8%).

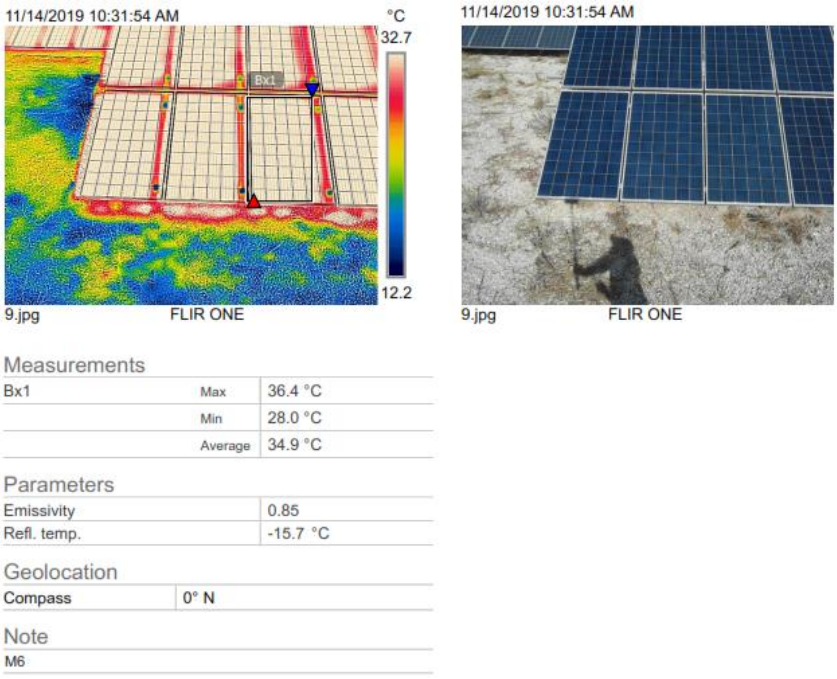

Fig. 10. An infrared thermal image was taken from each modules of the string.

Table 3. Experimental outline to determine the contribution of each module in output power of a string.

Experiment No : 22-42	**Module type: sunowe270w-polycrystaline**		**location of the cell : 6/D**		
Environmental conditions					
Cloud coverage (octa)	Wind speed (Bft)	Irradiation (W/m2)	Ambient temp (°C)	shading	Module cleanliness
0	1	865	23	no	Clean
Configuration and location of the thermographic camera					
Angle between camera and module surface (degree)	Distance between camera and cell (m)	Tilt of module (degree)	Current of module (A)	thermal stability (min)	
87	5.2	30	8.1	60	

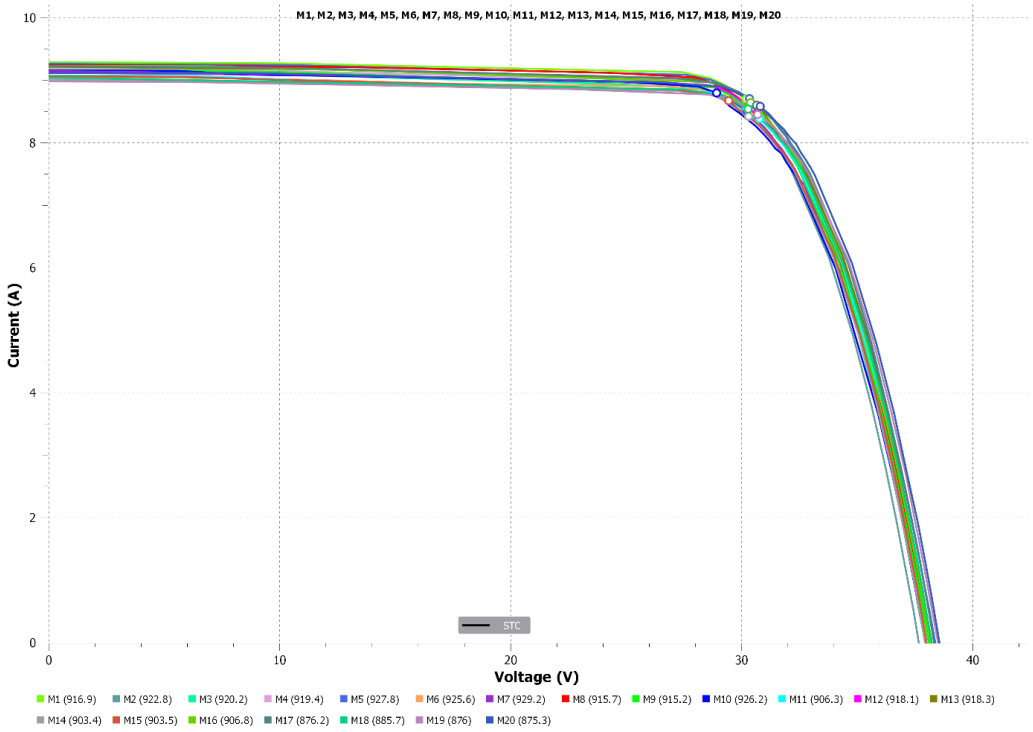

Fig. 11. I-V curves of 20 modules in string number 9.

5. Results and discussion

Ideally, according to the number of modules in the string (20 modules in string number 9), the contribution of each module should be 5%, but in practice, due to the different productions of the modules, the contribution of the modules in output power will be different. So the test results of I-V curve were analyzed and the contribution of each module in the output power of string number 9 were calculated. Then infrared images were analyzed and contribution of each module in output power were calculated by the computational method for three T_{margin} ($T_{margin} = 0\ °C$, $T_{margin} = 1\ °C$ and $T_{margin} = 3\ °C$). Then the results of computational method were compared with the results of the I-V curve test. For example based on the results of the I-V curve test, module number one delivered 257.58 w at the time of the test (the first line in table B.1), and therefore the contribution of this module in output power of string is equal to 5.039 percent. The results of computational method, for $T_{margin} = 0\ °c$, $T_{margin} = 1\ °c$ and $T_{margin} = 3\ °c$ is 5.13, 5.06 and 5%, respectively.

So according to test results (table B.1) for modules in which the difference between maximum and minimum temperature in STC conditions is less than 10 °C and therefore classified in terms of temperature pattern in the healthy group, the calculation of power contribution of each module through this method is very close to the actual value and have an error below 2.8%.

6. Conclusions

In this research, a computational method for determining the contribution of each module in the output power of a photovoltaic power plant was presented. The results of this research can be summarized as follows:

1. The best and most accurate way to calculate T_{ref} is to use a lambert radiator.

2. In normal conditions, 0.85 is the most accurate emissivity for the top glass of a photovoltaic module.

3. For modules in which the difference between maximum and minimum temperature in STC conditions is less than 10 °C and therefore classified in terms of temperature pattern in the healthy group, this computational method can analyze the infrared thermal image of the module and estimate the contribution of each module in output power of a string. The

results of this method is very close to the actual values (have an error below 2.8%) and the results are more accurate for $T_{margin} = 3\ ^{\circ}c$.

Declaration of Interest

The authors declared that there is no conflict of interest.

Acknowledgement

This article is part of my master's thesis entitled " Investigating the power contribution of each module in a photovoltaic system by using infrared thermography" which has been done and presented at the branch Faculty of Mechanical Engineering, Islamic Azad Univercity Khomeinishahr, Isfahan, Iran.

This research did not receive any specific grant from funding agencies in the public, commercial, or not-for-profit sectors.

References

[1] Köntges, M. et al., Performance and reliability of photovoltaic systems, Subtask Review of Failures of Photovoltaic Modules. IEA International Energy Agency (2014), IEA-PVPS T13-01:2014.

[2] Hoyer, U. et al., Analysis of PV modules by electroluminescence and IR thermography. In: 24th European Photovoltaic Solar Energy Conference (2009), pp. 3262 – 3266.

[3] Simon, M., L.Meyer, E., Detection and analysis of hot-spot formation in solar cells. Solar Energy Materials & Solar Cells (2010) 94, 106-113.

[4] A.Tsanakas, J., Ha, L., Buerhop, C., Faults and infrared thermographic diagnosis in operating c-Si photovoltaic modules. Renewable and Sustainable Energy Reviews (2016) 62, 695–709.

[5] Jaffery, Z. et al., Scheme for predictive fault diagnosis in photo-voltaic modules using thermal imaging. Infrared Physics & Technology (2017) 83, 182–187.

[6] Álvarez-Tey, G., Jiménez-Castañeda, R., Carpio, J., Analysis of the configuration and the location of thermographic equipment for the inspection in photovoltaic systems. Infrared Physics & Technology (2017) 87, 40–46.

[7] Takyi, G., Correlation of Infrared Thermal Imaging Results with Visual Inspection and Current-Voltage Data of PV Modules Installed in Kumasi, a Hot, Humid Region of Sub-Saharan Africa. Technologies (2017) *5*(4), 67.

[8] A Tsanakas, J., Botsaris, P., An infrared thermographic approach as a hot-spot detection tool for photovoltaic modules using image histogram and line profile analysis. The International Journal of Condition Monitoring (2012) 2, number1.

[9] user's manual FLIR Tolls/Tools+

[10] Moretón, R. et al., dealing in practice with hot spots. In: 29th European Photovoltaic Solar Energy Conference and Exhibition, (2014.).

[11] Gupta, R. et al., Application of Infrared Thermography for Non-Destructive Inspection of Solar Photovoltaic Modules, journal of none destructive testing and evaluation, (2017) 25-32.

[12] Mingyao, Ma. et al., Rapid diagnosis of hot spot failure of crystalline silicon PV module based on I-V curve. Microelectronics Reliability (2019) 100-101:113402.

[13] Berardone, I., Lopez Garcia, J., Paggi, M., Analysis of electroluminescence and infrared thermal images of monocrystalline silicon photovoltaic modules after 20 years of outdoor use in a solar vehicle. Solar Energy (2018) 173, 478–486.

[14] Gallardo-Saavedra, S., Hernández-Callejo, L., Duque-Perez, O., Technological review of the instrumentation used in aerial thermographic inspection of photovoltaic plants. Renewable and Sustainable Energy Reviews (2018) 93, 566–579.

[15] IEC Central Office, IEC62446-3, Photovoltaic (PV) systems – Requirements for testing, documentation and maintenance- Part 3: Photovoltaic modules and plants – Outdoor infrared thermography (2017).

[16] Giuseppina, C., Lo Brano, V., Moreci, E., Forecasting the Cell Temperature of PV Modules with an Adaptive System. International journal of photoenergy (2013)4.

[17]Köntges, M. et al., Review on Infrared and Electroluminescence Imaging for PV Field Applications. IEA International Energy Agency, IEA PVPS Task 13, Subtask 3.3 Report IEA-PVPS T13-10:2018 (2018).

Appendix A

The performance parameters of modules in the string number 9 are shown in table A.1

Table A.1. The test results of the module performance in string number 9.

IV curve Data	P_{mpp}				V_{oc}			V_{mpp}			I_{sc}			I_{mpp}		
String	MEAS w	STC w	NOM w	DIFF %	MEAS V	STC V	NOM V	MEAS V	STC V	NOM V	MEAS A	STC A	NOM A	MEAS A	STC A	NOM A
M1	221	263	270	2.7	34.6	38.1	38.0	27.4	30.2	31.1	8.60	9.29	9.15	8.05	8.70	8.68
M2	217	257	270	4.9	34.1	37.7	38.0	27.3	30.2	31.1	8.61	9.15	9.15	7.96	8.52	8.68
M3	216	256	270	5.1	34.3	37.9	38.0	27.5	30.4	31.1	8.50	9.14	9.15	7.86	8.44	8.68
M4	219	260	270	3.5	34.4	38.1	38.0	27.0	30.7	31.1	8.57	9.18	9.15	8.12	8.49	8.68
M5	224	264	270	2.2	34.7	38.4	38.0	27.4	30.3	31.1	8.70	9.26	9.15	8.16	8.70	8.68
M6	219	258	270	4.3	34.6	38.2	38.0	27.6	30.5	31.1	8.49	9.04	9.15	7.94	8.49	8.68
M7	219	257	270	4.7	34.4	38.0	38.0	27.4	30.2	31.1	8.56	9.11	9.15	7.98	8.51	8.68
M8	219	261	270	3.5	34.5	38.1	38.0	27.3	30.6	31.1	8.61	9.24	9.15	8.00	8.51	8.68
M9	216	259	270	4.0	34.5	38.1	38.0	27.4	30.3	31.1	8.44	9.16	9.15	7.89	8.56	8.68
M10	218	254	270	5.8	34.4	38.0	38.0	27.1	38.9	31.1	8.56	9.15	9.15	8.01	8.80	8.68
M11	214	258	270	4.4	34.7	38.2	38.0	27.9	30.8	31.1	8.32	9.08	9.15	7.69	8.39	8.68
M12	219	261	270	3.4	34.6	38.2	38.0	27.6	30.5	31.1	8.46	9.15	9.15	7.92	8.56	8.68
M13	220	263	270	2.6	34.7	38.2	38.0	27.7	30.6	31.1	8.51	9.21	9.15	7.94	8.60	8.68
M14	212	255	270	5.5	34.4	37.9	38.0	27.5	30.3	31.1	8.29	9.01	9.15	7.72	8.42	8.68
M15	212	255	270	5.5	34.4	38.0	38.0	27.5	29.4	31.1	8.29	9.06	9.15	7.72	8.67	8.68
M16	216	263	270	2.7	34.5	38.2	38.0	27.5	30.4	31.1	8.41	9.23	9.15	7.87	8.64	8.68
M17	210	264	270	2.4	34.6	38.3	38.0	27.5	30.6	31.1	8.16	9.23	9.15	7.61	8.60	8.68
M18	208	258	270	4.3	34.5	38.2	38.0	27.3	30.3	31.1	8.07	9.04	9.15	7.61	8.54	8.68
M19	207	259	270	3.9	34.7	38.5	38.0	27.6	30.7	31.1	7.97	8.98	9.15	7.50	8.45	8.68
M20	213	264	270	2.1	34.9	38.6	38.0	27.9	30.8	31.1	8.15	9.13	9.15	7.66	8.58	8.68

Appendix B

The contribution of each module in the output power of string number 9 is calculated by the computational method for three T_{margin} ($T_{margin} = 0\,°c$, $T_{margin} = 1\,°c$ and $T_{margin} = 3\,°c$) and are compared with the results of the I-V curve (performance curve) test. The results are given in Table B.1

Table B.1. The contribution of each module in output power of the string number 9.

Module number	Output power in operating conditions based on I-V curve (performance curve) testing	Contribution of power based on performance curve(%)	Contribution of power based on computational method $T_{margin} = 0\,°c$(%)	Error in computational method for $T_{margin} = 0\,°c$(%)	Contribution of power based on computational method $T_{margin} = 1\,°c$(%)	Error in computational method for $T_{margin} = 1\,°c$(%)	Contribution of power based on computational method $T_{margin} = 3\,°c$(%)	Error in computational method for $T_{margin} = 3\,°c$(%)
1	257.58	5.039	5.13	0.09	5.06	0.02	5	-0.04
2	252.72	4.944	5.07	0.12	5.06	0.11	5	0.06
3	253.53	4.960	5.10	0.14	5.06	0.10	5	0.04
4	255.96	5.007	5.11	0.10	5.06	0.05	5	-0.01
5	258.39	5.055	5.03	-0.02	5.02	-0.03	5	-0.05
6	255.96	5.007	5.03	0.02	5.03	0.02	5	-0.01
7	253.53	4.960	4.96	0	4.98	0.02	5	0.04
8	255.15	4.991	5.01	0.02	5.00	0.01	5	0.01
9	254.34	4.975	4.98	0.01	4.98	0.01	5	0.02
10	251.1	4.912	4.98	-0.02	4.93	0.02	5	0.09
11	254.34	4.975	5.03	0.06	5.02	0.04	5	0.02
12	257.58	5.039	4.95	-0.09	4.96	-0.08	5	-0.04
13	256.77	5.023	4.94	-0.08	4.95	-0.07	5	-0.02
14	253.53	4.960	4.93	-0.03	4.97	0.01	5	0.04
15	253.53	4.960	4.93	-0.03	4.97	0.01	5	0.04
16	257.58	5.039	4.97	-0.07	4.97	-0.07	5	-0.04
17	259.2	5.071	5.03	-0.04	5.02	-0.05	5	-0.07
18	255.15	4.911	4.92	-0.07	4.96	-0.03	5	0.01
19	256.77	5.023	4.97	-0.06	5.00	-0.02	5	-0.02
20	259.2	5.071	5.04	-0.04	5.00	-0.07	5	-0.07

Appendix C

The matrix of cell position in a single module is shown in figure C.1.

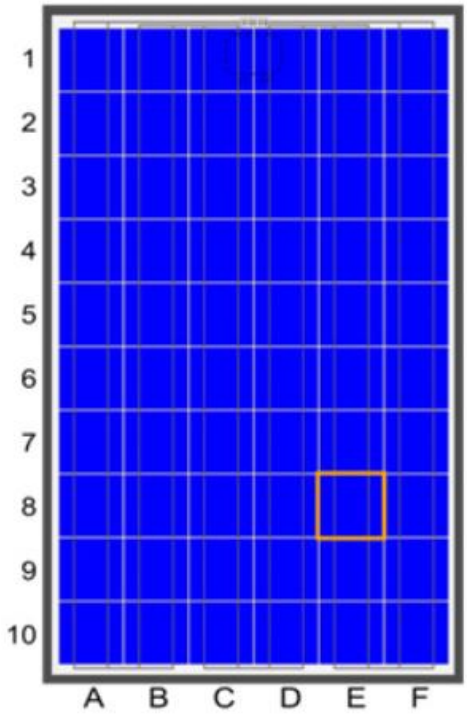

Fig. C.1. View for the designation of cell position, viewed from the front of a 60-cell module, with the junction box at the top (rear side). The marked cell is E/8 [15].